

Dynamics of the OH stretching mode in crystalline Ba(ClO₄)₂·3H₂O

Daniel Hutzler, Christian Brunner, Petko St. Petkov, Thomas Heine, Sighart F. Fischer, Eberhard Riedle, Reinhard Kienberger, and Hristo Iglev

Citation: *The Journal of Chemical Physics* **148**, 054307 (2018); doi: 10.1063/1.5007040

View online: <https://doi.org/10.1063/1.5007040>

View Table of Contents: <http://aip.scitation.org/toc/jcp/148/5>

Published by the [American Institute of Physics](#)

Articles you may be interested in

[Water adsorbate phases on ZnO and impact of vapor pressure on the equilibrium shape of nanoparticles](#)

The Journal of Chemical Physics **148**, 054701 (2018); 10.1063/1.5016122

[Perspective: Ab initio force field methods derived from quantum mechanics](#)

The Journal of Chemical Physics **148**, 090901 (2018); 10.1063/1.5009551

[Delocalization and stretch-bend mixing of the HOH bend in liquid water](#)

The Journal of Chemical Physics **147**, 084503 (2017); 10.1063/1.4987153

[Insight into ethylene interactions with molybdenum suboxide cluster anions from photoelectron spectra of chemifragments](#)

The Journal of Chemical Physics **148**, 054308 (2018); 10.1063/1.5008264

[A real-time extension of density matrix embedding theory for non-equilibrium electron dynamics](#)

The Journal of Chemical Physics **148**, 054108 (2018); 10.1063/1.5012766

[IR spectral assignments for the hydrated excess proton in liquid water](#)

The Journal of Chemical Physics **146**, 154507 (2017); 10.1063/1.4980121

PHYSICS TODAY

WHITEPAPERS

ADVANCED LIGHT CURE ADHESIVES

Take a closer look at what these environmentally friendly adhesive systems can do

READ NOW

PRESENTED BY
 MASTERBOND
ADHESIVES | SEALANTS | COATINGS

Dynamics of the OH stretching mode in crystalline $\text{Ba}(\text{ClO}_4)_2 \cdot 3\text{H}_2\text{O}$

Daniel Hutzler,¹ Christian Brunner,¹ Petko St. Petkov,² Thomas Heine,² Sighart F. Fischer,¹ Eberhard Riedle,³ Reinhard Kienberger,¹ and Hristo Iglev^{1,a)}

¹Physik-Department, Technische Universität München, James-Frank-Strasse, D-85748 Garching, Germany

²Wilhelm-Ostwald-Institut für Physikalische und Theoretische Chemie, Universität Leipzig, Linnéstraße 2, D-04103 Leipzig, Germany

³Lehrstuhl für BioMolekulare Optik, Ludwig-Maximilians-Universität München, Oettingenstraße 67, D-80538 München, Germany

(Received 29 September 2017; accepted 19 January 2018; published online 7 February 2018)

The vibrational dynamics of the OH stretching mode in $\text{Ba}(\text{ClO}_4)_2$ trihydrate are investigated by means of femtosecond infrared spectroscopy. The sample offers plane cyclic water trimers in the solid phase that feature virtually no hydrogen bond interaction between the water molecules. Selective excitation of the symmetric and asymmetric stretching leads to fast population redistribution, while simultaneous excitation yields quantum beats, which are monitored via a combination tone that dominates the overtone spectrum. The combination of steady-state and time-resolved spectroscopy with quantum chemical simulations and general theoretical considerations gives indication of various aspects of symmetry breakage. The system shows a joint population lifetime of 8 ps and a long-lived coherence between symmetric and asymmetric stretching, which decays with a time constant of 0.6 ps. *Published by AIP Publishing.* <https://doi.org/10.1063/1.5007040>

I. INTRODUCTION

In recent years, the crystal hydrates of organic and inorganic compounds have been extensively studied in order to work out the physical and biological properties of hydrogen bonds (H-bonds).^{1–5} Water oligomers bound in hydrate crystals offer confined water molecules in fixed geometrical arrangements in which environment and degree of confinement can be well adjusted by choosing the appropriate salt. The accessible range spans from quasi-isolated water molecules in monohydrates, via small water clusters up to well-separated two-dimensional water layers.^{2,5–9} The crystal structure of a great number of salt hydrates is well documented and stored in accessible databases,¹⁰ aiding the design and interpretation of experimental investigations. Even though the overall character of the interactions, such as electrostatic or H-bond interaction, in these systems equals that in the bulk, their relative importance can differ widely.^{11–14}

Previous measurements on hydrates focused on the large impact that different types of H-bonding have on the properties of aqueous systems.^{6,7,15,16} Here, we present a system that offers clusters of three water molecules that feature virtually no H-bonding between the individual water molecules. Generally, the contribution of the different interactions to the total energy in water trimers strongly depends on the angles between the three water molecules.^{17,18} While previous studies on these systems focused on the gas phase,^{19,20} we present first infrared (IR) pump–probe studies on coupled H_2O trimers in the solid state. $\text{Ba}(\text{ClO}_4)_2$ trihydrate offers well-separated two-dimensional water layers that contain plane cyclic water trimers. The H_2O molecules forming a three-membered ring

exhibit weak H-bonds to the oxygen atoms of the perchlorate ions, while there are practically no H-bonds among the individual water molecules. The weak H-bonds between water molecules and perchlorate anions have been noted before^{5,21} and their properties in aqueous perchlorate solutions attracted particular scientific interest.^{22,23} The high polarizability of the Ba^{2+} yields strong vibrational excitonic coupling between the OH stretching modes of two trimers contained in successive water layers, which are symmetry related by inversion on the nearest Ba^{2+} ion. This facilitates the interpretation of our experimental data with regard to delocalization of the OH stretching mode and can untangle differences in the overtone spectra of $\text{Ba}(\text{ClO}_4)_2 \cdot 3\text{H}_2\text{O}$ and quasi-isolated water molecules in $\text{NaClO}_4 \cdot \text{H}_2\text{O}$.

The OH stretching region in $\text{Ba}(\text{ClO}_4)_2$ trihydrate is investigated by time-resolved IR spectroscopy, augmented by steady-state IR measurements. The experimental data are in accordance with quantum simulations that demonstrate vibrational delocalization over coupled water trimers. The symmetric and asymmetric character is maintained upon delocalization and nature and phase of the vibrations can, to a large extent, be interpreted within the framework of the S_6 point group. We report on relaxation dynamics between symmetric and asymmetric stretching and quantify the corresponding exchange rate. Moreover, a joint vibrational lifetime of the two vibrations is extracted from the transient data. The mutual coherence of symmetric and asymmetric stretching is deduced from the decay of quantum beats that are observed via a combination tone predominating in the overtone spectrum.

II. EXPERIMENTAL DETAILS

The laser setup used to perform the time-resolved measurements was recently described in full detail.^{24,25} Here,

^{a)}Author to whom correspondence should be addressed: hristo.iglev@ph.tum.de

only some relevant parameters are summarized. The mid-IR pump pulses are generated by optical parametric amplification (OPA) with pre-amplification in the visible spectral range. The OPA process is pumped by 300 μJ pulses at a wavelength of 778 nm and a duration of 150 fs (CPA 2010; Clark MXR) and delivers tunable mid-IR pulses with energies on the microjoule level. The probe pulses are generated in a one-stage OPA pumped by 100 μJ . Extreme broadband pulses of spectral widths up to 900 cm^{-1} at 10% level [full width at half maximum (FWHM) of 400 cm^{-1}] and pulse energies of several hundred nanojoule are produced. Note that the pump and probe pulses in the setup have passively stabilized carrier envelope phase (CEP).²⁴ For a more precise excitation and to avoid spectral overlap, the bandwidth of the pump pulses can be controlled by the help of a $4f$ grating spectral selector. The pump pulses applied in this study are shown in Figs. 2(c), 2(d), and 4(b). All applied pulses are close to the Fourier limit at pulse durations of roughly 180 to 320 fs for pump and 50 fs for probe (time-bandwidth products of about 0.5).²⁴ After passing the sample, the probe beam is spectrally resolved in a polychromator (Chromex 250is) and recorded on a 32-channel infrared HgCdTe detector (IR-3216; Infrared Systems Development, Inc.). The spectral resolution of the system is 5 cm^{-1} .

The pump induced dynamics are monitored as the change in the optical density $\Delta OD = -\log(T/T_0)$ with T being the probe beam's transmission through an excited sample and T_0 being the transmission through an unexcited sample, i.e., with pump beam blocked. Usually, these dynamics include transient changes in the region of the ground state transition ($0 \rightarrow 1$) and of the excited state absorption (ESA) ($1 \rightarrow 2$). The former includes three time-dependent contributions: (i) ground state bleaching (GSB) for positive pump-probe delay times, (ii) perturbed free induction decay at negative delay time,²⁶ and (iii) spectral interference between the CEP-stable pump and probe pulses for positive and negative delays.²⁴ The overlap of these three processes makes the GSB data analysis very

challenging. By contrast, the anharmonicity of the OH stretching vibration leads to a redshift of the excited state absorption (ESA), yielding more direct information on the vibrational dynamics.

Steady state absorption spectra of the sample are recorded with a commercial TENSOR 27 Fourier-transform IR (FTIR, Bruker Optics) spectrometer that allows a spectral resolution of 0.5 cm^{-1} .

The sample is obtained from crystallization of a saturated solution of $\text{Ba}(\text{ClO}_4)_2$ dissolved in tridistilled H_2O . The hydrate crystals are grown by slowly cooling the salt solution between two CaF_2 windows in an evacuated cryostat. All the following measurements were conducted at a sample temperature of 200 K. Due to the low solubility of $\text{Ba}(\text{ClO}_4)_2$, a pronounced ice phase forms along the hydrate crystal leading to a polycrystalline structure of the sample. However, pump-probe measurements at delay times up to 1 ns show no transient heating of the hydrate phase after excitation of the ice phase and vice versa. This observation indicates that despite the polycrystalline nature of the present sample, the vibrational dynamics of the hydrate and ice phase can be investigated individually.²

III. RESULTS AND DISCUSSION

A. Crystal structure and vibrational spectrum

The crystal structure of $\text{Ba}(\text{ClO}_4)_2$ trihydrate is known from X-ray diffraction analysis.^{21,27,28} It forms a hexagonal crystal structure within space group $P6_3/m$ with two molecules per unit cell. The structure is schematically drawn in Fig. 1(b). Planes containing H_2O molecules are well separated by adjacent planes consisting of Ba^{2+} and ClO_4^- ions. Each perchlorate anion is bound to nine water molecules by weak hydrogen bonds (see next paragraph).²¹ The distance between two successive water layers is 483 pm. The top view in Fig. 1(c) shows that three water molecules (red) arrange circularly around a barium ion (purple) with an O–O distance of 284 pm, which is

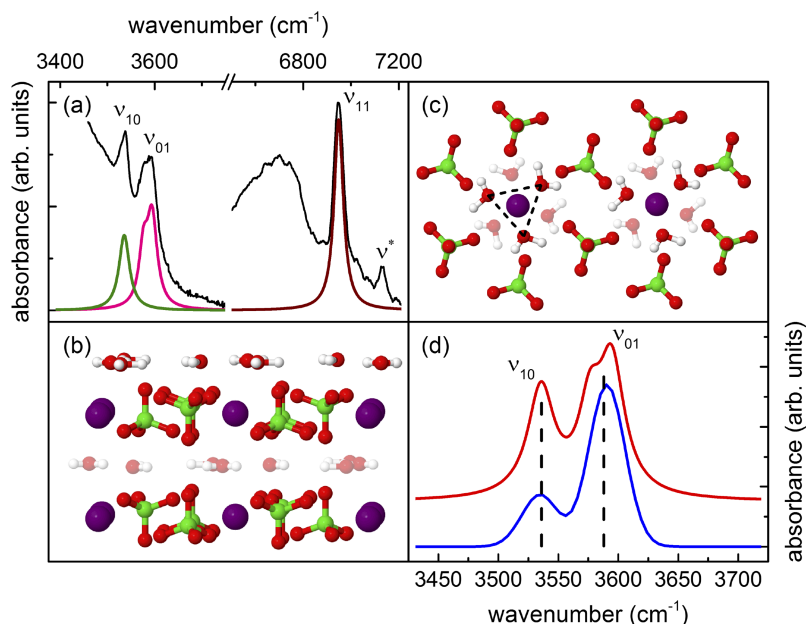


FIG. 1. (a) Normalized FTIR absorption spectrum of the OH stretching fundamental and overtone region in $\text{Ba}(\text{ClO}_4)_2$ trihydrate at 200 K (black line). Hydrate absorption bands of symmetric (green) and asymmetric stretching (pink) and their combination tone (brown) are modeled by Lorentzian distributions. An additional ice phase yields broad ice absorption bands in the spectra of fundamentals and overtones. Spectra in the two ranges were recorded with samples of varying thickness and have independently been normalized, and thus their absolute amplitudes cannot be put in relation. (b) Crystal structure of $\text{Ba}(\text{ClO}_4)_2$ trihydrate (Ba in purple, Cl in green, H in white, and O in red). Planes consisting of water molecules alternate with planes comprised of salt ions. (c) Top view of the crystal structure shown in Fig. 1(b). Water trimers placed behind one another are twisted by an angle of 60° (opaque and transparent red) and arrange cyclic around a Ba^{2+} ion in the center. (d) Background corrected stretching bands (red), ν_{10} and ν_{01} , and corresponding absorption spectrum deduced from density functional theory (DFT) calculations (blue). The data are vertically stacked for better visualization.

very similar to the corresponding oxygen distance in bulk water and ice.²⁹ This validates the use of the term trimer even though the three water molecules exhibit practically no H-bonding amongst each other. The trimer in the water level below [transparent red in Fig. 1(c)] shows an angular displacement of 60°. Note that alternatively the non-centrosymmetric space group $P6_3$ has also been considered. Our investigations point to the presence of non-centrosymmetric features, which are due to either static disorder or dynamic coupling to symmetry breaking low-frequency modes.

The Badger-Bauer relation,^{21,30} which assumes that the shift of the stretching frequency is proportional to the H-bond enthalpy, can be used for a rough estimation of the H-bond strength in the hydrate. Here we compare the OH frequency in isotopically mixed ice and $\text{Ba}(\text{ClO}_4)_2 \cdot (\text{HDO} + 2\text{D}_2\text{O})$ hydrate (see Fig. S1 of the [supplementary material](#)). The large amount of blue-shift between the hydrate peak (at 3564 cm^{-1}) and the center of the ice absorption (at 3304 cm^{-1}) gives evidence of relatively weak H-bonds between water molecules and perchlorate anions.^{31–33} More precisely, the vapor-crystal shift of ice at 273 K is 401 cm^{-1} ,²¹ while the corresponding shift of $\text{Ba}(\text{ClO}_4)_2$ -trihydrate is only 141 cm^{-1} . As the enthalpy of sublimation of ice at 273 K is 6.1 kcal/mol per H-bond, the Badger-Bauer relation gives 2.1 kcal/mol as a rough estimation of the H-bond strength between water and the perchlorate ion.

An FTIR spectrum of the sample at 200 K is shown in Fig. 1(a). Due to the low solubility of $\text{Ba}(\text{ClO}_4)_2$, a pronounced ice phase forms along the hydrate crystal and gives rise to a broad ice absorption band centered around 3300 cm^{-1} . The two sharp features at 3536 cm^{-1} and 3588 cm^{-1} are due to the H_2O molecules bound in the hydrate crystal.²¹ Note that comparable measurements in $\text{Ba}(\text{ClO}_4)_2 \cdot (\text{HDO} + 2\text{D}_2\text{O})$ reveal an absorption band at 3564 cm^{-1} that is centered between the two features in the H_2O data (see Fig. S1 of the [supplementary material](#)). This indicates that the two peaks in Fig. 1(a) can be assigned to symmetric and asymmetric stretching. In the following, the vibrational states are denoted as ν_{sa} with s being the quantum number of symmetric stretching and a that of asymmetric stretching. It is emphasized that this notation only relates to individual water molecules and does not pertain to the symmetry assumptions regarding the hydrate crystal. The asymmetric band ν_{01} is composed of two sub-bands at 3576 cm^{-1} and 3595 cm^{-1} with full widths at half maximum (FWHMs) of 23 cm^{-1} and 26 cm^{-1} , while the symmetric band ν_{10} at 3536 cm^{-1} can be well reproduced by a single Lorentzian peak with a FWHM of 27 cm^{-1} . However, measurements at lower temperatures show the onset of a splitting of ν_{10} as well.

For better visualization of the hydrate features, the ice contribution was subtracted in the red curve in Fig. 1(d). The blue curve is the result of quantum-chemical simulations (see the [supplementary material](#) for details) that yield a semiclassical combination of normal modes. For better comparison, the computed frequencies are scaled by a factor of 0.977. In accordance with the above assignment of the two hydrate features, the calculated modes exhibit exclusively symmetric or asymmetric character within the respective band. Due to the imposed $P6_3/m$ symmetry, the modes are fully delocalized and do not reproduce the splitting of the asymmetric stretching

band in the experimental data. For two trimers located in planes on top of each other [opaque and transparent red molecules in Fig. 1(c)], the calculations reveal that pairs of water molecules placed on opposite sides of a barium cation vibrate either in phase or out of phase. The respective phase relation is valid for all three water pairs, indicating strong coupling between neighboring trimers.

The overtone region shown in Fig. 1(a) exhibits two pronounced hydrate features on top of the broadband absorption of the ice fraction around 6700 cm^{-1} : a prominent band at 6949 cm^{-1} and a smaller peak at 7130 cm^{-1} denoted by ν^* . It is consistent with the time-resolved experiments below and the expected anharmonicity to assign the peak at 6949 cm^{-1} to the combination band ν_{11} of symmetric and asymmetric stretching. By contrast, the spectra of isolated D_2O molecules³⁴ and quasi-isolated water molecules in $\text{NaClO}_4 \cdot \text{H}_2\text{O}$ (see Fig. S2 of the [supplementary material](#)) exhibit two additional features due to the overtones of symmetric and asymmetric stretching, ν_{20} and ν_{02} .

B. Anharmonic couplings and localization

In the following we want to discuss the observed splitting of ν_{01} . This band points towards anharmonic coupling and breakage of the $P6_3/m$ inversion symmetry since the side-band is not seen in the calculated spectrum [Fig. 1(d)]. The structure provides interesting information for this task. Each perchlorate ion has a partner symmetry related by reflection on the water plane. Out-of-plane motion of the hydrogen atoms or wagging motion of water trimers modulates the OH bond distance between the two perchlorate partners. Contrary to observed bond exchange in aqueous solution,²³ an ideal crystal restrains the motion. In solution, transitions between states with minor energy differences can be bridged by the short-range coupling of collision-like processes. In a crystal, one needs coupling to energy matching low frequency modes. For reversible motion of the hydrogen between both symmetry related bonding partners, a saddle point located on the water plane would be predicted. Such specification based on symmetry considerations can help us to find modes, which promote the bond exchange motion. It could also shed light on the so-called “angular jump exchange kinetic model.”²³ Moreover, it is orientation selective in the induced polarization response³⁵ and frequency selective in the dielectric response.²² The challenge is to combine the symmetry considerations with the localization dynamics, since the local amplitudes of fully delocalized vibrations would be too small to cause local bond exchange processes.

To get insight into localization dynamics on a trimer, we extended the unit cell to include two $\text{Ba}(\text{ClO}_4)_2 \cdot 3\text{H}_2\text{O}$ units. We found a strong IR active wagging mode of the trimers, induced via motion of the perchlorate ions against the Ba^{2+} (see Movie S1 of the [supplementary material](#)). Interestingly, a finite displacement along this normal mode coordinate leads to the $P6_3$ space group, which has been discussed as alternative to $P6_3/m$ in the literature.^{27,28} The motion of this mode affects the effective charge on the hydrogen. This in turn modulates the force constants for the stretching motion and can cause the splitting of the ν_{01} band. The simulation of such low frequency

dynamics is challenging due to the fact that curved coordinates based on force fields of valence coordinates are needed, to avoid unphysically large third order coupling terms of the stretching motion and the overtones of bending modes. A perturbation expansion up to 5th order is required in the Cartesian coordinate system to reduce these discrepancies. This conclusion is based on studies on smaller systems³⁶ but is relevant for anharmonic coupling between low frequency bending modes and OH stretching modes in general.

Taking the information from steady-state and time-resolved spectroscopy (discussed in Sec. III C), we conclude that the inversion on Ba^{2+} can be violated due to static disorder and low frequency modes as considered above. It turns out that a consistent interpretation of the transient spectra is possible, if we assume that the same mode that causes the splitting also steers the localization dynamics. In particular we relate the observed sub-picosecond dynamics to localization of the delocalized vibration on to an excitation on water trimers. This relaxation evolves within 0.5 ps, the time corresponding to half a period of the inversion symmetry breaking mode. This way we can understand that the overtones ν_{20} and ν_{02} are symmetry forbidden for $\text{Ba}(\text{ClO}_4)_2 \cdot 3\text{H}_2\text{O}$ in the $P6_3$ space group and for the C_{3h} group of a trimer as well. Interestingly, the transition into the combination band is not symmetry forbidden. Note that corresponding experiments on $\text{NaClO}_4 \cdot \text{H}_2\text{O}$ do not show the sideband of ν_{01} but they show the diagonal overtones ν_{20} and ν_{02} . This is expected for the excitation on isolated water molecules due to diagonal anharmonic coupling of the stretching modes.

Furthermore, we interpret the weak ν^* band as transition into the unrelaxed superposition of ν_{10} and ν_{01} and the more strongly allowed transition from ν_{10} or ν_{01} to ν_{11} as transitions into the relaxed band ν_{11} . Excitation from an unrelaxed state corresponding to a vertical Franck-Condon like transition can also explain the appearance of a frequency shift in the transient data [see Fig. 4(a)]. On the same time scale, a relaxation towards an equilibrated population between the two stretching modes is observed for the time delayed spectra (see Fig. 2). We conclude that the relaxation into the relaxed fully localized eigenstate ν_{11} can proceed in three steps. During the first step,

the excited state configuration reorganizes, which is better seen in ν_{01} . As a result, the inversion symmetry on Ba^{2+} gets lost and the excitation localizes on one trimer. This is necessary to develop large amplitude motion for the formation of a H-bond. In the following, coherent motion along the reaction coordinate evolves, which finally results in a partial localization of the H-bond to one out of plane partner. This process can be observed via the transition to the combination band. Finally, relaxation to the ground state takes place via coupling to overtones of the OH stretching to the overtones of OH bending modes.

C. Time-resolved spectroscopy

1. Selective excitation of the symmetric and asymmetric stretching vibration

In three individual experiments, mid-IR excitation pulses were applied to pump the ground state transitions of the symmetric stretch ($\nu_{00} \rightarrow \nu_{10}$), the asymmetric stretch ($\nu_{00} \rightarrow \nu_{01}$), and both simultaneously ($2\nu_{00} \rightarrow \nu_{10} + \nu_{01}$). The spectral profiles of the pump pulses used in the different experiments are illustrated by the green lines in Figs. 2(c), 2(d), and 4(b). The sample absorption spectrum is also shown in black for comparison. Here, the slightly split asymmetric mode is considered as one absorption band centered at 3588 cm^{-1} with an effective spectral width of 42 cm^{-1} . This is reasonable since the spectral width of the pump pulses exceeds the energy separation of the two sub-bands by far. The pump induced dynamics is monitored through the excited state absorption (ESA). The transient data, measured with various probe polarizations, do not show a systematic dependence on the relative pump-probe polarization conditions (data not shown). Therefore, the linear polarizations of both beams are kept parallel throughout this study. All of the following measurements were conducted at 200 K. The transient data below are not corrected for minor contributions from the ice band.

Transient spectra recorded after selective excitation of ν_{01} at 3588 cm^{-1} are plotted in Fig. 2(a). The curves exhibit two distinct features at $3355 \pm 5\text{ cm}^{-1}$ and $3403 \pm 5\text{ cm}^{-1}$. At a pump-probe delay of 0.5 ps, the former shows the

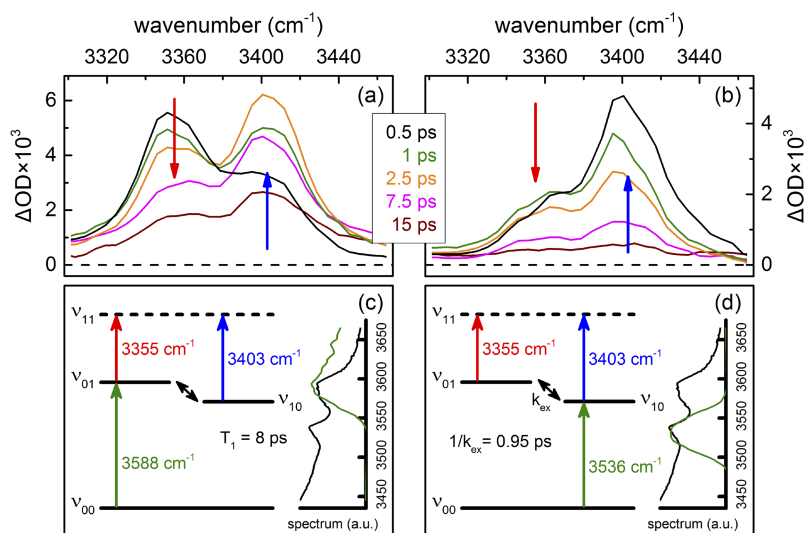


FIG. 2. (a) Transient spectra recorded in $\text{Ba}(\text{ClO}_4)_2$ trihydrate at several delay times after pumping ν_{01} at 3588 cm^{-1} . Red and blue arrows indicate the maxima of the ESAs at 3355 cm^{-1} and 3403 cm^{-1} . (b) Corresponding spectra recorded after excitation of ν_{10} at 3536 cm^{-1} . [(c) and (d)] Energy schemes for both excitation conditions. Pump excitation is illustrated as green arrows. Red and blue arrows represent the probed ESAs. Black arrows indicate relaxation between ν_{10} and ν_{01} . k_{ex} is the effective exchange rate. T_1 represents the excited state population lifetime. The spectral profiles of the applied pump pulses are illustrated by the green curves, while the sample absorption is shown in black for comparison.

larger amplitude, while 2.5 ps after excitation the feature at 3403 cm^{-1} is more pronounced. Spectra recorded at longer delays show no appreciable change in their spectral shape and display a joint overall decay of the signal. The FWHM of the two peaks is $40 \pm 5\text{ cm}^{-1}$ and their energy separation of roughly 52 cm^{-1} is very similar to that between the two hydrate peaks shown in Fig. 1(a). Figure 2(b) shows data measured after selectively pumping ν_{10} , with the spectral profile of the applied pump pulse illustrated in Fig. 2(d). At a delay time of 0.5 ps, the absorption band at 3403 cm^{-1} is very pronounced. Subsequently, its high energy wing slightly shifts to smaller energies and the second feature at 3355 cm^{-1} becomes more dominant. Spectra obtained at delays larger than 2.5 ps show similar shape and dynamics as in Fig. 2(a).

Based on the above data, the energy schemes depicted in Figs. 2(c) and 2(d) are deduced. Pumping the asymmetric stretching ν_{01} yields direct excitation of the left branch in Fig. 2(c), while the absorption at 3403 cm^{-1} evolves with some delay. In Fig. 2(d), the right branch associated with the symmetric stretching is directly pumped and the feature at 3355 cm^{-1} occurs with temporal delay. Following the excited pathways in Figs. 2(c) and 2(d) the total frequency in both cases lies at roughly the same value of $6940 \pm 5\text{ cm}^{-1}$. The latter agrees well with the combination band in Fig. 1(a) and corroborates that ν_{11} actually is a combination tone. Note that the initial redshift of the high energy wing in Fig. 2(b) and the associated change in the energy distance between ν_{10} and ν_{11} is likely a signature of the aforementioned localization of the OH stretching mode.

Figure 3(a) shows transients measured in the maximum of the two absorption bands after excitation of ν_{01} . One clearly sees that the peak at 3355 cm^{-1} is present immediately after pumping, while the transient recorded at 3405 cm^{-1} exhibits a slower and well-resolved rise time. In accordance with the above observations, the dynamics indicates that the $\nu_{01} \rightarrow \nu_{11}$ transition is directly excited, while the $\nu_{10} \rightarrow \nu_{11}$ ESA occurs only after population redistribution between ν_{01} and ν_{10} . Corresponding dynamics recorded after excitation at ν_{10} is shown in Fig. 3(b). Here, the absorption at 3390 cm^{-1} can be directly accessed and fully develops within 0.3 ps, followed by a decay within the first few picoseconds. Note that this transient was taken left of the actual maximum in order to

suppress the influence of the initial spectral shift of the high energy wing [see Fig. 2(b)]. The transient at 3355 cm^{-1} rises more slowly. For delay times exceeding 2.5 ps, all four curves in Figs. 3(a) and 3(b) show approximately the same dynamics, yielding an overall population lifetime of $T_1 = 8 \pm 1\text{ ps}$. The extracted relaxation time is an order of magnitude larger than the respective times found in bulk water and ice;^{37,38} however, it is not surprising for stretching modes of very weak to non-hydrogen bonded OH groups.^{2,5,34,39}

Next, the exchange rate k_{ex} for relaxation between symmetric and asymmetric stretching shall be extracted. Since the blue and red transients in Figs. 3(a) and 3(b) show the same long time kinetics, they can be scaled to lie on top of each other at large pump-probe delays [dotted lines in Figs. 3(c) and 3(d)]. By subtracting the scaled blue trace from the red one, the slower population dynamics proceeding with $k = 1/T_1$ can be removed. In doing so, the $\nu_{10} \leftrightarrow \nu_{01}$ dynamics can be obtained from the yielded difference curves, which are given in black in Figs. 3(c) and 3(d). For more details on the used kinetic model, see the [supplementary material](#). The two transients are in good accordance and picture a monoexponential decay proceeding with a total rate of $(0.85 \pm 0.15\text{ ps})^{-1}$. Since the exchange dynamics is overlaid with the decay of the total population, the latter rate equals $k_{ex} + k$. From this, one can directly calculate k_{ex} to be $(0.95 \pm 0.2\text{ ps})^{-1}$.

A detailed look on the data presented in Fig. 3(c) shows a small deviation between data points and fit at 1.7 ps and 3.4 ps. Comparison to additional data measured after direct excitation of the asymmetric stretching mode indicates that these deviations are due to periodic modulation with central frequency of about 20 cm^{-1} . The excellent agreement of this number with the energy separation between the two asymmetric sub-bands points towards a possible beating between these sub-bands.

2. Simultaneous excitation of the symmetric and asymmetric stretching vibration

Finally, a broad pump pulse was applied to simultaneously excite the symmetric and asymmetric stretching mode [see green and black curves in Fig. 4(b)]. Corresponding transient spectra are depicted in Fig. 4(a). At 0.15 ps, two absorption bands are present. The high energy feature subsequently shifts

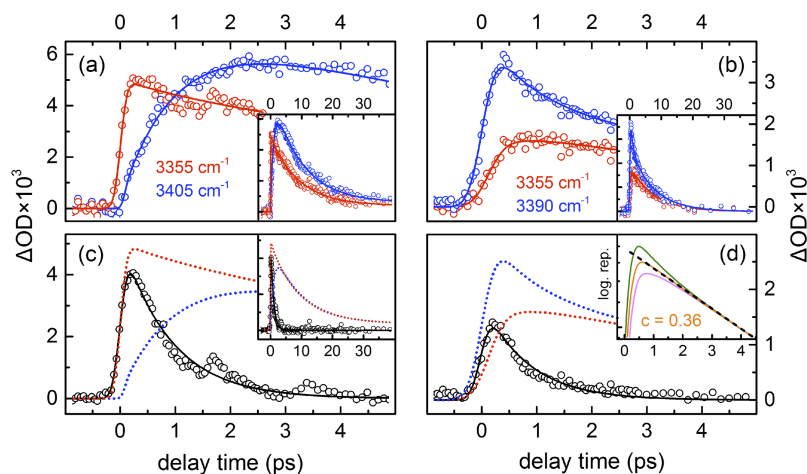


FIG. 3. (a) Time evolution of the $\nu_{01} \rightarrow \nu_{11}$ and $\nu_{10} \rightarrow \nu_{11}$ transition recorded at 3355 cm^{-1} and 3405 cm^{-1} after excitation of ν_{01} . (b) Corresponding data measured at 3355 cm^{-1} and 3390 cm^{-1} after excitation at ν_{10} . (c) Scaled transients (red and blue dotted lines) and resulting differential signals (black) of the data in (a). (d) Respective transients calculated for the data in (b). The inset shows the corresponding sum curves computed for scaling factors c of 0.1 (magenta), 0.36 (orange), and 1 (green). Note that the sum curves are normalized to coincide at long delay times.

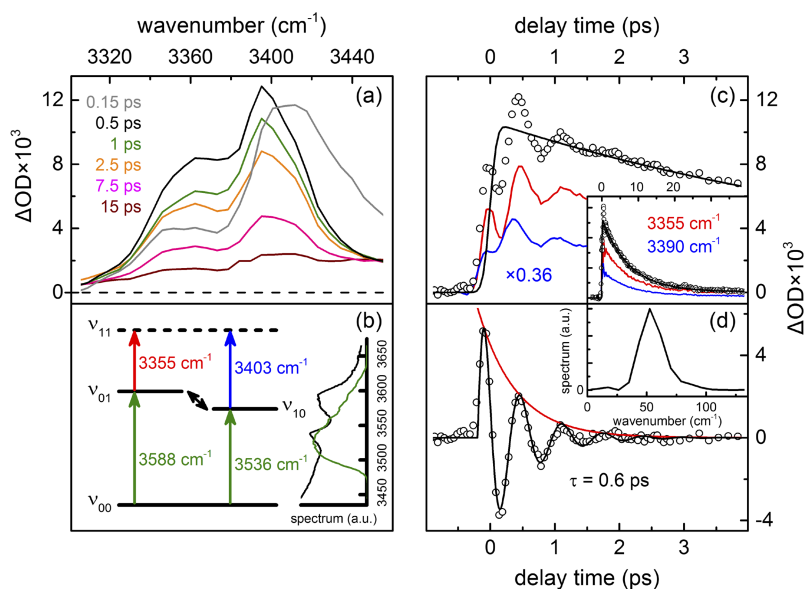


FIG. 4. (a) Transient spectra recorded at several delay times after simultaneous excitation of symmetric and asymmetric stretching in $\text{Ba}(\text{ClO}_4)_2$ trihydrate. (b) Corresponding energy scheme, pump spectrum (green curve), and sample absorption (black). Pump excitation is indicated by green arrows, ESAs by red and blue arrows, and relaxation between ν_{10} and ν_{01} by a black arrow. (c) Transients measured at 3355 cm^{-1} (red) and 3390 cm^{-1} (blue). The blue curve is scaled by a factor of 0.36. Black circles depict the sum signal of blue and red traces. The black line represents an exponential decay associated with the population relaxation time T_1 . (d) Quantum beat signal extracted by subtracting the fit from the sum curve in Fig. 3(c). The fitted black line is comprised of an initially chirped sine overlaid with a monoexponential decay (red). τ denotes the coherence lifetime. The power spectrum of the beating signal is shown in the inset.

to smaller energies. At delay times exceeding 1 ps, the transient spectra exhibit similar shape and dynamics as in the measurements shown in Figs. 2(a) and 2(b). The small offset on the high energy side of the spectra can be referred to a temperature dependent absorption change in the ice absorption band. The associated energy scheme is drawn in Fig. 4(b). Inspecting the blue (already scaled by a factor c , see below) and red transients in Fig. 4(c), one immediately sees a sinusoidal modulation on top of the two curves that is interpreted as a quantum beating between ν_{10} and ν_{01} observed via the mutual final state ν_{11} . For a more detailed analysis of this phenomenon, first the fast dynamics due to k_{ex} shall be removed from the data. Since the two transients are directly proportional to the populations of ν_{10} and ν_{01} , appropriate scaling and subsequent summation of both curves yield the total excited state population. The latter only decays with $T_1 = 8$ ps, while the $\nu_{10} \leftrightarrow \nu_{01}$ exchange dynamics is cut out (see the [supplementary material](#) for more details).

The inset in Fig. 3(d) demonstrates how this is done in practice. First, the blue curve is multiplied by a factor c . Subsequently, the scaled blue and red transients are added up. If the scaling factor is chosen correctly, the sum transient represents the exponential decay of the total population. In a logarithmic representation, this decay is pictured by a straight line (black dashed), whose gradient reflects the population relaxation rate k . Minimizing the deviation of the sum curve from the dashed line yields the correct value of the scaling factor c . In the inset in Fig. 3(d), obviously the orange line with $c = 0.36$ fits best. Since the two transients in Fig. 4(c) were measured at the same frequencies of 3355 cm^{-1} and 3390 cm^{-1} , here the same scaling factor can be applied and one obtains the sum data indicated by black circles. The latter shows a monoexponential decay with a lifetime of 8 ± 1 ps (same as for individual excitation) overlaid with the above mentioned periodical modulation.

Figure 4(d) shows the signal remaining after subtracting a fit of the population decay (black solid line) from the total curve in Fig. 4(c). It can be well approximated by a sine wave

multiplied by an exponential decay. However, a detailed data analysis shows that the sinusoidal modulation exhibits a shift towards smaller frequencies within the first few hundred femtoseconds. This was incorporated into the fitting procedure. The resulting curve is shown as black line in Fig. 4(d). It is the product of an exponential decay with a time constant of 0.6 ps (red line) and a sine with an initial frequency of 85 cm^{-1} that reduces exponentially to 54 cm^{-1} with a time constant of 0.5 ps and subsequently stays constant. The fitted curve agrees very well with the experimental data. The power spectrum of the measured beating signal is illustrated in the inset of Fig. 4(d). This spectrum shows a maximum around 54 cm^{-1} , which agrees with the energy distance between ν_{10} and ν_{01} . The broadening to higher frequencies agrees with the assumed initial frequency shift from 85 cm^{-1} to 54 cm^{-1} . This spectral shift is of the same nature as the shift in Fig. 2(b) and can also be related to the localization dynamics after symmetry breaking. According to this assumption, the symmetry breaking occurs with a time constant of about 0.5 ps. However, distinctly assigning the frequency shift in the beat signal to the symmetry breaking requires further experimental proof.

The decay of the beat signal is a measure of the loss of coherence between ν_{10} and ν_{01} . From the red slope in Fig. 4(d), a coherence decay time τ of 0.60 ± 0.07 ps is extracted. The smallest linewidth involved in the asymmetric stretching, which pertains to the low-energy sub-band, exhibits a bandwidth of 23 cm^{-1} . Without even accounting for the linewidth of the symmetric stretching, this value already yields a dephasing time below 0.5 ps and therewith smaller than the coherence decay time. This points towards strong correlation of the frequency fluctuations of ν_{10} and ν_{01} . Prolonged coherences like that have been reported in 2D electronic spectroscopy measurements. Here, vibronic coupling is proposed as the underlying mechanism.^{40,41} In particular, the coupling to vibrational modes, which are resonant with the energy gaps between the electronic excitations, is emphasized.^{42,43} In accordance to these findings, the coupling to low-lying vibrations with

energies matching the gap between ν_{10} and ν_{01} is suggested as the origin of the long-lived coherence in $\text{Ba}(\text{ClO}_4)_2$ trihydrate. A possible mode has been related to symmetry breaking above.

IV. CONCLUSION

In conclusion, we report femtosecond pump-probe measurements on the excited states of the OH stretching vibration in cyclic H_2O trimers in the crystalline phase. After individual excitation of the asymmetric stretching, a relaxation into the symmetric stretching was observed and vice versa. The time constant of this fast population redistribution is 0.95 ± 0.2 ps. Moreover, a population relaxation time T_1 of 8 ± 1 ps was obtained from the overall decay of the signal. Simultaneous excitation of ν_{10} and ν_{01} yielded quantum beats that were observed via a combination tone ν_{11} that is predominant in the overtone spectrum. On theoretical grounds, we show that information from steady-state and time resolved spectroscopy applied to crystalline systems can contribute to the microscopic understanding of the primary relaxation processes. Vibrational spectroscopy is capable to detect eigenstates including anharmonic couplings or to identify localized states. In our specific case, an OH stretching overtone ν_{11} could be localized on a trimer by breaking the inversion symmetry. The observed transient downshift of the beating frequency with a time constant of about 0.5 ps was tentatively assigned to this process. Moreover, from the decay of the beat signal a long-lived coherence with a lifetime of 0.60 ± 0.07 ps is extracted. The observation points to Fermi resonance mixing including coupling to combination bands with low frequency out of plane modes. Here we tried to identify such a mode. Its particular crystal structure makes the presented $\text{Ba}(\text{ClO}_4)_2$ trihydrate a well-suited system to study vibrationally induced symmetry breakage and prolonged coherences of the OH stretching mode.

SUPPLEMENTARY MATERIAL

See [supplementary material](#) for Movie S1, Figs. S1–S3, methods, and Refs. 44–49.

ACKNOWLEDGMENTS

The financial support by the Deutsche Forschungsgemeinschaft (DFG) Cluster of Excellence “Munich-Center of Advanced Photonics (MAP)” is gratefully acknowledged.

The authors declare no competing financial interests.

- ¹M. Mascal, L. Infantes, and J. Chisholm, “Water oligomers in crystal hydrates—What’s news and what isn’t?,” *Angew. Chem., Int. Ed.* **45**, 32–36 (2006).
- ²S. Pandelov, B. M. Pilles, J. C. Werhahn, and H. Iglev, “Time-resolved dynamics of the OH stretching vibration in aqueous NaCl hydrate,” *J. Phys. Chem. A* **113**, 10184–10188 (2009).
- ³B. A. Zakharov, B. A. Kolesov, and E. V. Boldyreva, “Monitoring selected hydrogen bonds in crystal hydrates of amino acid salts: Combining variable-temperature single-crystal x-ray diffraction and polarized Raman spectroscopy,” *Phys. Chem. Chem. Phys.* **13**, 13106–13116 (2011).
- ⁴B. A. Zakharov and E. V. Boldyreva, “Reversible pressure-induced disordering in bis (DL-serinium) oxalate dihydrate,” *J. Mol. Struct.* **1078**, 151–157 (2014).

- ⁵D. Hutzler, J. C. Werhahn, R. Heider, M. Bradler, R. Kienberger, E. Riedle, and H. Iglev, “Highly selective relaxation of the OH stretching overtones in isolated HDO molecules observed by infrared pump–repump–probe spectroscopy,” *J. Phys. Chem. A* **119**, 6831–6836 (2015).
- ⁶J. C. Werhahn, S. Pandelov, S. S. Xantheas, and H. Iglev, “Dynamics of weak, bifurcated, and strong hydrogen bonds in lithium nitrate trihydrate,” *J. Phys. Chem. Lett.* **2**, 1633–1638 (2011).
- ⁷W. J. Smit and H. J. Bakker, “Vibrational energy relaxation of water molecules in a hydrated lithium nitrate crystal,” *J. Phys. Chem. C* **120**, 11078–11084 (2016).
- ⁸L. J. Barbour, G. W. Orr, and J. L. Atwood, “An intermolecular (H_2O)₁₀ cluster in a solid-state supramolecular complex,” *Nature* **393**, 671–673 (1998).
- ⁹M. Zuhayra, W. U. Kampen, E. Henze, Z. Soti, L. Zsolnai, G. Huttner, and F. Oberdorfer, “A planar water tetramer with tetrahedrally coordinated water embedded in a hydrogen bonding network of $[\text{TC}_4(\text{CO})_{12}(\mu_3\text{-OH})_4\cdot 4\text{H}_2\text{O}]$,” *J. Am. Chem. Soc.* **128**, 424–425 (2006).
- ¹⁰F. H. Allen, “The cambridge structural database: A quarter of a million crystal structures and rising,” *Acta Crystallogr., Sect. B: Struct. Sci.* **58**, 380–388 (2002).
- ¹¹R. Ludwig, “Water: From clusters to the bulk,” *Angew. Chem., Int. Ed.* **40**, 1808–1827 (2001).
- ¹²K. Liu, J. D. Cruzan, and R. J. Saykally, “Water clusters,” *Science* **271**, 929–933 (1996).
- ¹³S. S. Xantheas, “Cooperativity and hydrogen bonding network in water clusters,” *Chem. Phys.* **258**, 225–231 (2000).
- ¹⁴F. N. Keutsch and R. J. Saykally, “Water clusters: Untangling the mysteries of the liquid, one molecule at a time,” *Proc. Natl. Acad. Sci. U. S. A.* **98**, 10533–10540 (2001).
- ¹⁵H. D. Lutz, “Structure and strength of hydrogen bonds in inorganic solids,” *J. Mol. Struct.* **646**, 227–236 (2003).
- ¹⁶F. Zhang, K. Li, H. Ratajczak, and D. Xue, “Hydrogen bonds in inorganic crystals: A microscopic study on the valence electron distribution of hydrogen in O–H ··· O systems,” *J. Mol. Struct.* **976**, 69–72 (2010).
- ¹⁷G. Chal, M. M. Szczesniak, P. Cieplak, and S. Scheiner, “*Ab initio* study of intermolecular potential of H_2O trimer,” *J. Chem. Phys.* **94**, 2873–2883 (1991).
- ¹⁸F. N. Keutsch, J. D. Cruzan, and R. J. Saykally, “The water trimer,” *Chem. Rev.* **103**, 2533–2578 (2003).
- ¹⁹N. Pugliano and R. J. Saykally, “Measurement of quantum tunneling between chiral isomers of the cyclic water trimer,” *Science* **257**, 1937–1940 (1992).
- ²⁰S. S. Xantheas and T. H. Dunning, Jr., “The structure of the water trimer from *ab initio* calculations,” *J. Chem. Phys.* **98**, 8037–8040 (1993).
- ²¹G. Brink and M. Falk, “Infrared studies of water in crystalline hydrates: $\text{NaClO}_4\cdot\text{H}_2\text{O}$, $\text{LiClO}_4\cdot 3\text{H}_2\text{O}$, and $\text{Ba}(\text{ClO}_4)_2\cdot 3\text{H}_2\text{O}$,” *Can. J. Chem.* **48**, 2096–2103 (1970).
- ²²K. J. Tielrooij, N. Garcia-Araez, M. Bonn, and H. J. Bakker, “Cooperativity in ion hydration,” *Science* **328**, 1006–1009 (2010).
- ²³M. Ji, M. Odelius, and K. J. Gaffney, “Large angular jump mechanism observed for hydrogen bond exchange in aqueous perchlorate solution,” *Science* **328**, 1003–1005 (2010).
- ²⁴M. Bradler, J. C. Werhahn, D. Hutzler, S. Fuhrmann, R. Heider, E. Riedle, H. Iglev, and R. Kienberger, “A novel setup for femtosecond pump–repump–probe IR spectroscopy with few cycle CEP stable pulses,” *Opt. Express* **21**, 20145–20158 (2013).
- ²⁵M. Bradler, C. Homann, and E. Riedle, “Mid-IR femtosecond pulse generation on the microjoule level up to 5 μm at high repetition rates,” *Opt. Lett.* **36**, 4212–4214 (2011).
- ²⁶P. Hamm, “Coherent effects in femtosecond infrared spectroscopy,” *Chem. Phys.* **200**, 415–429 (1995).
- ²⁷S. Ramaseshan and N. Mani, “The crystal structure of barium perchlorate trihydrate $\text{Ba}(\text{ClO}_4)_2\cdot 3\text{H}_2\text{O}$ and the crystal coordination of Ba^{++} ion,” *Z. Kristallogr. - Cryst. Mater.* **114**, 200–214 (1960).
- ²⁸J. C. Gallucci and R. E. Gerkin, “Structure of barium perchlorate trihydrate,” *Acta Crystallogr., Sect. C: Crystal Struct. Commun.* **44**, 1873–1876 (1988).
- ²⁹U. Bergmann, A. Di Cicco, P. Wernet, E. Principi, P. Glatzel, and A. Nilsson, “Nearest-neighbor oxygen distances in liquid water and ice observed by x-ray Raman based extended x-ray absorption fine structure,” *J. Chem. Phys.* **127**, 174504-1–174504-5 (2007).
- ³⁰R. M. Badger and S. H. Bauer, “Spectroscopic studies of the hydrogen bond. II. The shift of the O–H vibrational frequency in the formation of the hydrogen bond,” *J. Chem. Phys.* **5**, 839–851 (1937).

- ³¹D. Eisenberg and W. Kauzmann, *The Structure and Properties of Water* (Oxford University Press, 1969).
- ³²F. Franks, *Water: A Comprehensive Treatise*, Vol. 1 (Plenum Press, New York, 1972).
- ³³G. E. Walrafen, "Raman spectral studies of the effects of perchlorate ion on water structure," *J. Chem. Phys.* **52**, 4176–4198 (1970).
- ³⁴D. B. Wong, C. H. Giammanco, E. E. Fenn, and M. D. Fayer, "Dynamics of isolated water molecules in a sea of ions in a room temperature ionic liquid," *J. Phys. Chem. B* **117**, 623–635 (2013).
- ³⁵C. Greve, N. K. Preketes, R. Costard, B. Koeppe, H. Fidder, E. T. J. Nibbering, F. Temps, S. Mukamel, and T. Elsaesser, "N–H stretching modes of adenosine monomer in solution studied by ultrafast nonlinear infrared spectroscopy and *ab initio* calculations," *J. Phys. Chem. A* **116**, 7636–7644 (2012).
- ³⁶S. F. Fischer and A. Irgens-Defregger, "Vibrational relaxation pathways in C₂H₂ and C₂D₂," *J. Phys. Chem.* **87**, 2054–2059 (1983).
- ³⁷S. Woutersen, U. Emmerichs, H. K. Nienhuys, and H. J. Bakker, "Anomalous temperature dependence of vibrational lifetimes in water and ice," *Phys. Rev. Lett.* **81**, 1106 (1998).
- ³⁸R. L. A. Timmer and H. J. Bakker, "Vibrational Förster transfer in ice Ih," *J. Phys. Chem. A* **114**, 4148–4155 (2010).
- ³⁹H. Graener and G. Seifert, "Vibrational and orientational relaxation of monomeric water molecules in liquids," *J. Chem. Phys.* **98**, 36–45 (1993).
- ⁴⁰V. Tiwari, W. K. Peters, and D. M. Jonas, "Energy transfer: Vibronic coherence unveiled," *Nat. Chem.* **6**(3), 173–175 (2014).
- ⁴¹L. Wang, G. B. Griffin, A. Zhang, F. Zhai, N. E. Williams, R. F. Jordan, and G. S. Engel, "Controlling quantum-beating signals in 2D electronic spectra by packing synthetic heterodimers on single-walled carbon nanotubes," *Nat. Chem.* **9**, 219–225 (2017).
- ⁴²A. W. Chin, J. Prior, R. Rosenbach, F. Caycedo-Soler, S. F. Huelga, and M. B. Plenio, "The role of non-equilibrium vibrational structures in electronic coherence and recoherence in pigment-protein complexes," *Nat. Phys.* **9**(2), 113–118 (2013).
- ⁴³J. Lim, D. Paleček, F. Caycedo-Soler, C. N. Lincoln, J. Prior, H. Von Berlepsch, S. F. Huelga, M. B. Plenio, D. Zigmantas, and J. Hauer, "Vibronic origin of long-lived coherence in an artificial molecular light harvester," *Nat. Commun.* **6**, 1–7 (2015).